Fachtagung "Lasermethoden in der Strömungsmesstechnik"
8. – 10. September 2015, Dresden

Simultaneous density and velocity field measurements by means of combined differential interferometry and Long-range Micro-PIV

S. Kordel, T. Nowak, R. Skoda and J. Hussong
Chair of Fluid Machinery, Ruhr-Universität Bochum, 44801 Bochum, Germany

Schlagworte: Fernfeld-µPIV, Differential Interferometrie, Konvektion
Key words: Long-range µPIV, Differential Interferometry, Convection

Abstract

In the present study Long-range Micro Particle Image Velocimetry (µPIV) and Differential Interferometry (DI) are combined in a novel manner to enable both simultaneous measurements of the velocity field and the depth-integrated scalar field using the same laser pulse for both recordings. The interference technique is robust against vibrations and allows quantifying density, temperature, pressure or concentration distributions in various transient flow problems such as natural convection, turbulent mixing or hydrodynamic cavitation. In the present work, transient velocity and density gradient fields could be successfully determined in a temperature driven boundary layer flow resolving density gradients of 0.03 $\frac{kg}{m^3 mm}$ corresponding temperature gradients of 0.15 $\frac{K}{mm}$.

Introduction

Early studies on simultaneous density and velocity field measurements were utilized by Skarman et al. [1]. They combined holographic interferometry with 3D-PTV measurements to capture the temperature and flow field with the same camera. To separate particle images from image background fringes, two consecutive recordings were deducted from each other. As a result, the same tracer appeared as bright and dark spot in the same image making a straight forward PIV processing by means of autocorrelation impossible [2]. Winklhofer et al. carried out simultaneous pressure and velocity measurements by combining Mach-Zehnder Interferometry and 1D Molecular Tagging Velocimetry (MTV) [3]. However, for MTV two different illumination wave lengths have to be used to discriminate the interference and the MTV signal. Furthermore, for 2D MTV more complex laser-created grid pattern are required [4]. In the current work such technical challenges are avoided by combining PIV rather than MTV with interferometric measurements.
The interferometric measurement principle utilizes the Lorenz-Lorentz relation to link refractive index changes to spatial or temporal density or temperature gradients in the fluid. Refractive index gradients lead to phase changes of light rays passing the measurement section which can be deducted from the resulting interference pattern in the image plane [5]. The most common interference techniques for flow problems are the Mach-Zehnder Interferometry (MZI) and the Shearing Interferometry also referred to as Differential Interferometry (DI) [6]. While interference techniques are often used to measure density or pressure fields in gas flows, applications to weakly compressible liquid flows are scarce [7]. Iben et al. performed pressure field measurements in cavitating flows by means of Mach-Zehnder Interferometry [8]. However, utmost care has to be taken to match the object and the reference beam for Mach-Zehnder Interferometry when pulsed lasers of short coherence lengths are chosen or vibrating systems

are investigated. Therefore, in the present work the Differential Interferometry technique is employed to measure depth-integrated temperature gradient fields.
In the current work we show how Long-range Micro Particle Image Velocimetry and Differential Interferometry can be combined in one set-up to use the same laser pulse of a standard double-pulsed Nd:YAG Laser for simultaneous velocity and density gradient field measurements.

Methods

Experimental Set-up

Optical System and components

Fig. shows a schematic drawing of the experimental set-up. A frequency-doubled dual cavity Nd:YAG laser (Litron Nano) is used for both µPIV and Differential Interferometry measurements at 5 Hz recording frequency.

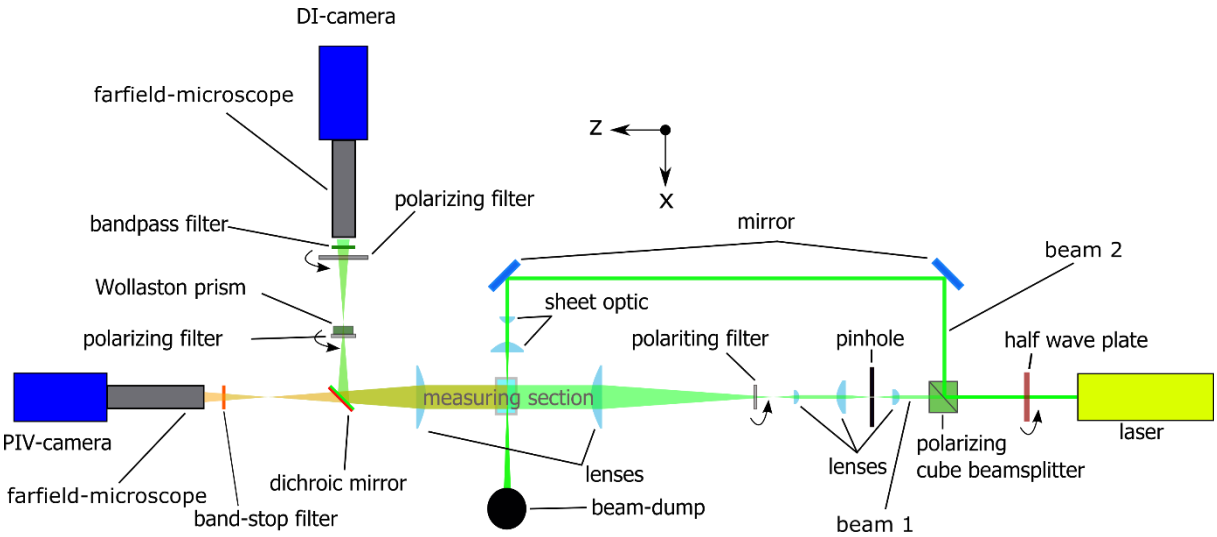

Fig. 1: Schematic of combined Long-range µPIV and Differential Interferometry

For this, each laser pulse of approximately 65 mJ is split into two separate beams of approximately 95 % and 5 % laser intensity by combining a half wave plate and a polarizing beam splitter. The first optical beam path (beam 1) with low laser intensity passes a spatial filter system while propagating the z-axis to ensure a uniform Gaussian intensity profile. Afterwards the divergent laser beam is focused to a parallel ray beam. The second beam path (beam 2) is guided into the measurement section from a 90 degree angle (light rays propagating in x-direction) to excite suspended, Rhodamine B coated fluid tracers of 25.07 µm nominal diameter (Microparticles GmbH). Both, the fluorescence signal of the particles and the laser light are separated behind the measurement section by a dichroic mirror for distinct µPIV and DI recordings. While the fluorescence signal of tracers passes the dichroic mirror, the laser light is deflected and passes two polarization filters and a Wollaston prism, the main parts of the differential interferometer, which create the interference fringes in the image plane. The signals are recorded by two separate 12 bit CCD-cameras (Imager pro SX, LaVision) of 2456 x 2058 pixel. By using two farfield microscopes (Infinity K2, DistaMax) with a 2x magnification, a spatial resolution of 1.58 µm/pixel is reached for both recordings. This yields to a field of view of 3.246 mm x 3.874 mm.

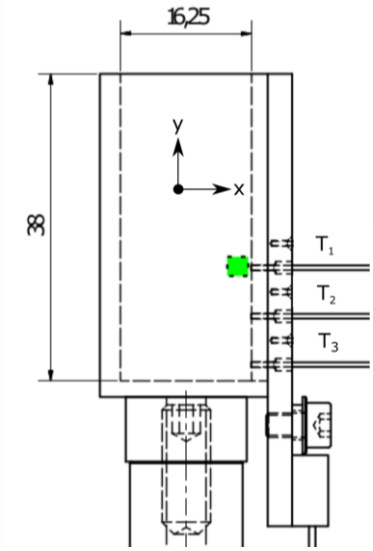

Fig. 2: Cuvette with heated side wall and VOW

Measurement Section

Measurements are done in a closed optical cuvette (Altmann Analytics) as shown in Fig. 2. One sidewall is replaced with a brass plate and heated by a 10 Ω resistor in combination with a 4 W power supply. Thermocouples are placed inside the brass plate along the y-axis with 2 mm, 8 mm and 14 mm spacing from the bottom wall of the cuvette. These thermocouples reach slightly into the water allowing to measure the water temperature at approximately 0.2 mm spacing from the brass plate surface.

Measurement Procedure

For each measurement sequence a time series of 300 double images is recorded at 5 Hz recording frequency with both cameras. This results in a total recording time of 60 s. A sufficient particle displacement of approximately 10 was reached at the end of the time series for an interframing time of dt = 5 ms. Experiments show that the particle concentration is limited due to an increasing background noise in the DI recordings. Therefore, the seeding density was limited to 78 ppm. After the filling process, the cuvette is closed to avoid a free surface. To get a good spatial resolution in the DI recordings a high number of fringes is demanded. In the current set-up this distance is limited reaching a number of 12 fringes within the Region of Interest (ROI) with a fringe width of approximately 140 pixels. This leads to a spatial resolution of 438 µm. By rotating the Wollaston prism the orientation of the fringes can be adapted. All measurements are done with an orientation angle of ~ 45 ° between the fringe axis and the brass plate surface. To account for the background flow induced during the filling process a time sequence of 2 s was recorded immediately before heating the brass plate at its bottom end with 4 Watt. The resulting time dependent temperature distribution inside the plate and the liquid is recorded with the 3 thermocouples (T_1 *to* T_3) as indicated in Fig. 2.

Evaluation Procedure

Differential Interferometry

The evaluation of the fringe pattern resulting from the interference measurements includes the image preprocessing, the fringe detection and calculation of the phase shift distribution due to temperature induced refractive index gradients in the flow. The main processing steps are illustrated in Fig. 3 a-h.
Firstly, a min-max filter is applied to all raw images with an edge length larger than the fringe width (l = 180 pixel) as shown in Fig. 3 b). Secondly, the salt and pepper noise in the image is reduced by a sliding minimum filter with an edge length of 11 pixels (see Fig. 3 c). Consequently, the image is converted into a binary image before processing (Fig. 3 d). An additional median filter with a window size of 15 x 15 pixels smoothes the fringe edges (Fig. 3 e).

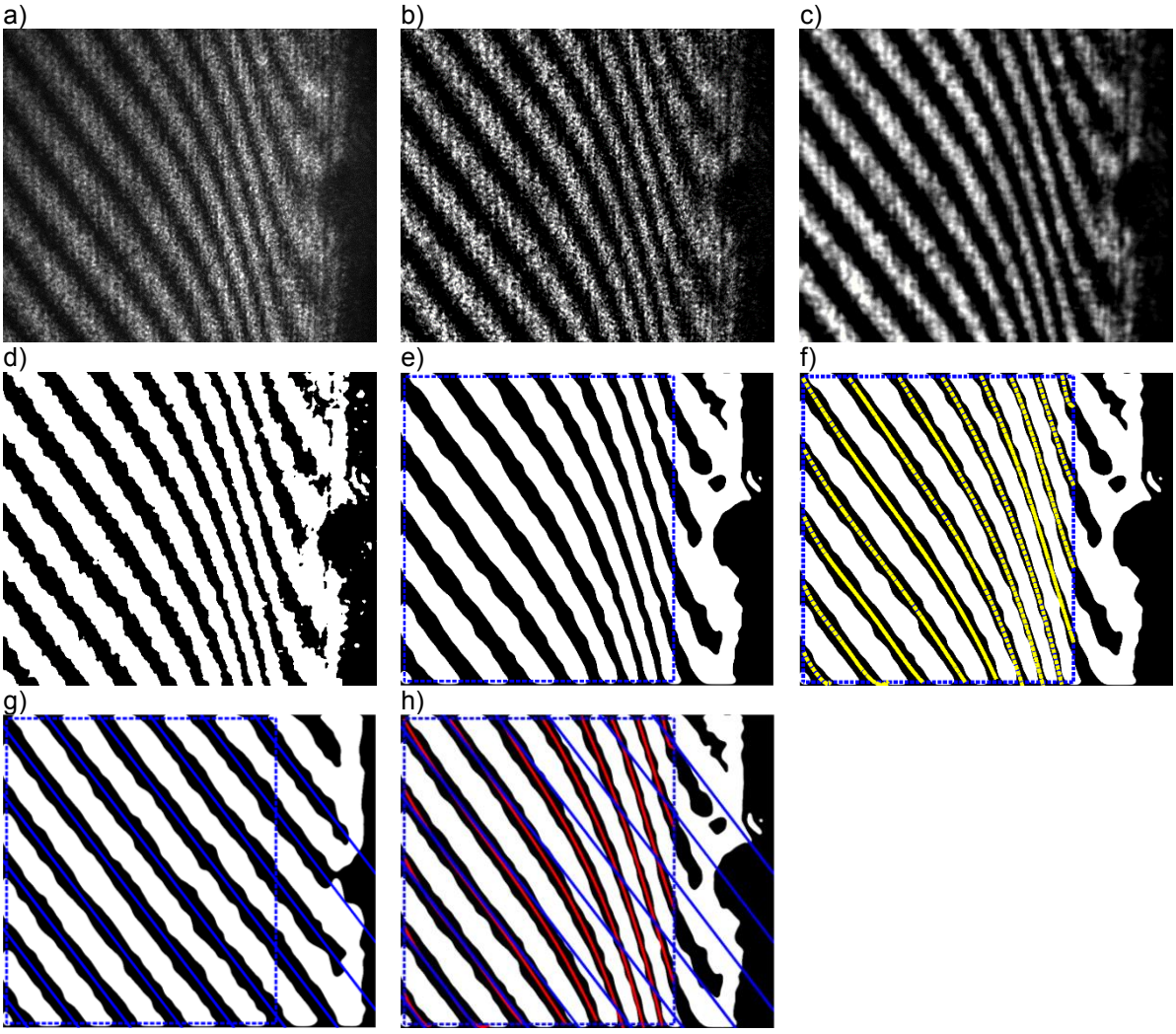

Fig. 3: Image processing steps of DI images a) raw image, b) min-max filter, c) subtracted sliding minimum, d) binary image, e) median filter, f) fringe pattern with indicated confidence intervals of fitting curves within the ROI, g) reference fringe pattern before heating, h) superposed warped image and reference image

In a subsequent step all destructive interference pattern are identified as separate objects. Within the region of interest as indicated in Fig. 3 e) for each fringe its centerline position on the ROI borderline is determined.
A fourth order polynomial is fitted to each fringe. Since the position of each fringe on the borderline of the ROI is pre-determined, the initial position and slope are not open parameters any longer. Therefore only the curvature evolution is determined through a nonlinear fit, using the grey value information inside each object from the initial interference image (Fig. 3 b) as weighting factor for an improved fitting result. The confidence bounds of these fits are less than 12 pixels for all evaluated fringe pattern (s. Fig 3 f).

$$\frac{\partial \bar{\rho}(x,y)}{\partial \zeta} = \frac{\lambda}{Kbd}\frac{\Delta S(x,y)}{S} \tag{1}$$

For moderate temperature changes the density gradient normal to the initial fringe orientation $\frac{\partial \bar{\rho}(x,y)}{\partial \zeta}$ is directly proportional to the relative fringe displacement $\frac{\Delta S(x,y)}{S}$. Equation 1 describes the relation between the density gradient and the relative fringe displacement where λ is the wavelength of the light source, b = 5 mm is the depth of the measurement volume, d is the

distance of two interfering light beams and K is the Gladstone – Dale Constant of light at 532 nm wavelength in water at atmospheric pressure [9] .The fringe displacements are derived from the displacement Δs of the warped fringes from their original state before (Fig. 3 g) and during (Fig. 3h) the heating process, respectively. Using the confidence bounds of 12 pixels as minimum detectable displacement of a fringe, the minimum resolved density gradient can be estimated by Equation 1 with 0.03 $\frac{kg}{m^3 mm}$. Assuming linearity between density and temperature for this interval, the corresponding temperature gradient is 0.15 $\frac{K}{mm}$.

Long-range Micro PIV

The processing of the Long-range µPIV measurements is done with the commercial software DaVis 8.2.2 (LaVison GmbH). To improve the signal to noise ratio a sliding minimum filter is first applied to the particle images with a length scale of 3 pixels. Additionally, by subtracting the minimum with a sliding filter window of 20 pixels edge length, the signal to noise ratio is further improved. For all measurements a region of interest of 2.626 mm x 2.400 mm was depicted. The depth of field at the chosen magnification is 0.42 mm. For the vector calculation a 2D multi-pass cross correlation was chosen with a final interrogation window size of 128 x 128 pixel and 50 % overlapping. With a working distance of 490 mm and a calculated magnification of 2.17 the vector spacing is ~102 µm. In the region closer than 2.5 mm to the heated wall 9.5 % spurious vectors were deleted after a median test or in a peak ratio threshold test. For a peak ratio is less than 1.5, the vector was deleted. 0.5 % of the deleted vectors were replaced with 2nd or 3rd correlation peak. The remaining vectors were interpolated. In the region farther than 2.5 mm to heated wall particle displacement and therefore flow velocity was nearly zero. This causes bad correlation results and a high amount of spurious vectors.

Results and Discussion

Verification of the combined measurement technique

Combined Long-range µPIV and DI measurements could be verified for a series of measurements in which the influence of the measurement technique on the flow and the influence of the thermocouple on the boundary layer were tested. Fig. 4 a) and b) show a representative density gradient field and the corresponding velocity vector field 58 s after heating the brass sidewall inside the cuvette with 4 W. Fig. 4 a) shows the gradient field in ζ-direction as indicated, thus normal to the interference fringes which were oriented under 45° to the brass plate surface (s. Fig. 3 g). The maximum density gradient inside the chosen ROI was determined to 1.6 $\frac{kg}{m^3 mm}$ at a spacing to the wall of 0.8 – 0.9 mm, while it decreases to nearly zero within 2 mm distance to the wall. The corresponding velocity field is shown in Fig. 4 b). It shows maximum velocities of about 5.0 mm/s which occur approximately at 0.8 mm spacing from the heated side wall.

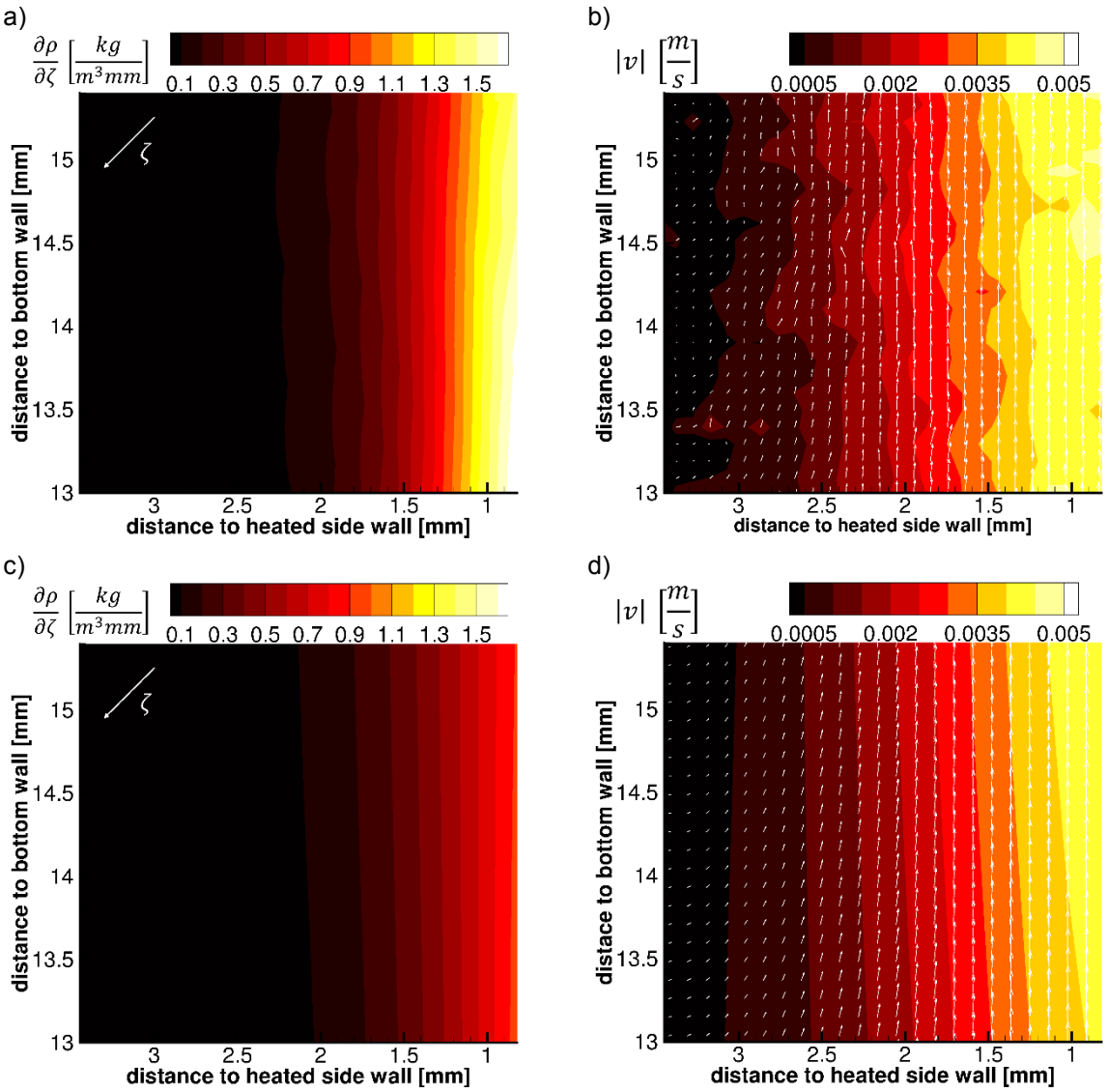

Fig. 4: results after 58 s heating a) density gradient field; b) measured velocity; c) simulated density gradient field; d) simulated velocity field

Qualitative comparison of experiments and simulations

Additionally to the measurements a numerical computation has been done using ANSYS CFX. The 3D Model consists of 1,080,000 notes resolving the hydraulic boundary layer with approximately 20 cells over its thickness. Since CFX utilizes an incompressible solver, density gradients were calculated using the International Steam Tables [9].
Fig. 4 c) shows the calculated density gradient field in ζ-direction. In Fig. 4 d) the corresponding velocity field is pointed out. In simulation one can see that the biggest gradients of about 0.9 to 1.0 $\frac{kg}{m^3 mm}$ are located approximately at a wall spacing of 0.8 – 0-9 mm. The maximum velocities in the ROI of 4.5 mm/s are reached.
In comparison to the measurement the simulated maximum velocity and density gradient are smaller. While the velocity fields are in good agreement with local deviations being below 5 %, local deviations in the density gradient field of up to 35 % are observed.

The authors anticipate that these predominately originate from deviations in the heat conduction properties of the brass plate in the simulations and experiments as the exact alloyed composition was unknown.

Measurement repeatability

Fig. 5 a) shows the mean density gradient field of an ensemble of 3 independent measurement campaigns. The standard deviation of the ensemble is illustrated in Fig. 5 b). Maximum deviations occur within 0.8 – 1 mm spacing to the heated wall. All deviations are less than 3.2 %. The corresponding temperature measurements of thermocouples T_1 – T_3 show a standard deviation of 5 % indicating that variations are mainly due to variations in the heating.

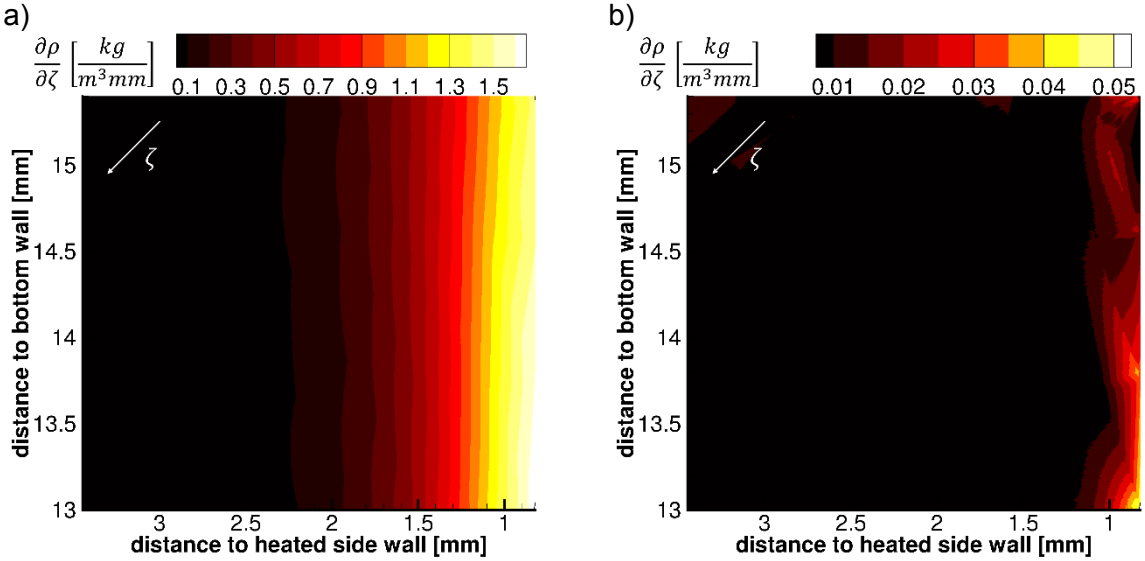

Fig. 5 a) mean density gradient field after 58 s of 3 measurement cycles; b) corresponding standard deviation

Conclusion and outlook

Long-range µPIV and Differential Interferometry could be successfully combined in a novel manner. The combined measurement technique was applied and verified on a temperature driven wall flow with the current set-up, respectively. Spatial resolutions of 438 µm and 102 µm for DI and Long-range µPIV were shown. DI measurements are well reproducible to within 3.2 % standard deviation even for small ensembles. µPIV measurements show good agreement with the simulation results. The corresponding local deviation is less than 5 %. Current DI measurements have a bigger difference with respect to current simulation results of up to 35 %. We anticipate that these differences originate from a mismatch in the heat conductivity used in simulation.

A modification of the set-up is required to further increase the spatial resolution of DI measurements by reducing the fringe spacing through optimized lens systems. The ability to capture density gradients directly at the wall is limited due to the double image created by the Wollaston prism. To capture density gradients at less than 190 µm spacing to the heated wall prisms with smaller divergence angles have to be used. However this affects the spatial resolution. Since

future investigations aim to investigate cavitation induced pressure waves in the flow an optimization for wall bounded investigations is beyond the goal of this study.
Further improvement steps include an optimized evaluation of velocity vectors by using variable interframing times for µPIV recordings.

Acknowledgements

This work was supported by funds of the Competence Center of Hydraulic Fluid Machinery.

Literature

[1] Skarman, B., Becker, J., & Wozniak, K. (1996). Simultaneous 3D-PIV and temperature measurements using a new CCD-based holographic interferometer. Flow Measurement and Instrumentation, 7(1), 1–6.

[2] Westerweel, J. (1997). Fundamentals of digital particle image velocimetry. Measurement Science and Technology, 8(12), 1379–1392.

[3] Winklhofer, E., Kull, E., Kelz, E., & Morozov, A. (2001). Comprehensive hydraulic and flow field documentation in model throttle experiments under cavitation conditions. In ILASS-Europe 2001, 17 International Conference on Liquid Atomization and Spray Systems.

[4] Koochesfahani, M., Cohn, R., MacKinnon, C., & Koochesfahani, M. (2000). Simultaneous whole-field measurements of velocity and concentration fields using a combination of MTV and LIF. Measurement Science and Technology, 11(9), 1289–1300.

[5] Merzkirch, W. (1987). Flow visualization (2. ed). Orlando: Acad. Press

[6] Egbers, C., Brasch, W., Sitte, B., Immohr, J., & Schmidt, J.-R. (1999). Estimates on diagnostic methods for investigations of thermal convection between spherical shells in space. Measurement Science and Technology, 10(10), 866–877.

[7] Woisetschläger, J., Pretzler, G., Jericha, H., Mayrhofer, N., & Pirker, H. P. (1998). Differential interferometry with adjustable spatial carrier fringes for turbine blade cascade flow investigations. Experiments in Fluids, 24(2), 102–109.

[8] Iben, U., Morozov, A., Winklhofer, E., & Wolf, F. (2011). Laser-pulse interferometry applied to high-pressure fluid flow in micro channels. Experiments in Fluids, 50(3), 597–611.

[9] Wagner, W., & Kretzschmar, H.-J. (2008). International Steam Tables. Berlin, Heidelberg: Springer Berlin Heidelberg.